

The University of Akron IdeaExchange@UAKron

Chemical and Biomolecular Engineering Faculty
Research

Chemical and Biomolecular Engineering
Department

7-1-2004

Local Oxidation of Metal and Metal Nitride Films

N Farkas

J. C. Tokash

G. Zhang

Edward A. Evans

University of Akron Main Campus, evanse@uakron.edu

R. D. Ramsier

See next page for additional authors

Please take a moment to share how this work helps you [through this survey](#). Your feedback will be important as we plan further development of our repository.

Follow this and additional works at: http://ideaexchange.uakron.edu/chemengin_ideas

 Part of the [Chemistry Commons](#)

Recommended Citation

Farkas, N.; Tokash, J. C.; Zhang, G.; Evans, Edward A.; Ramsier, R. D.; and Dagata, J. A., "Local Oxidation of Metal and Metal Nitride Films" (2004). *Chemical and Biomolecular Engineering Faculty Research*. 15.

http://ideaexchange.uakron.edu/chemengin_ideas/15

This Article is brought to you for free and open access by Chemical and Biomolecular Engineering Department at IdeaExchange@UAKron, the institutional repository of The University of Akron in Akron, Ohio, USA. It has been accepted for inclusion in Chemical and Biomolecular Engineering Faculty Research by an authorized administrator of IdeaExchange@UAKron. For more information, please contact mjon@uakron.edu, uapress@uakron.edu.

Authors

N Farkas, J. C. Tokash, G. Zhang, Edward A. Evans, R. D. Ramsier, and J. A. Dagata

Local oxidation of metal and metal nitride films

N. Farkas

Departments of Physics and Chemistry, The University of Akron, Akron, Ohio 44325

J. C. Tokash

Department of Physics, The University of Akron, Akron, Ohio 44325

G. Zhang and E. A. Evans

Department of Chemical Engineering, The University of Akron, Akron, Ohio 44325

R. D. Ramsier^{a)}

Departments of Physics, Chemistry, and Chemical Engineering, The University of Akron, Akron, Ohio 44325

J. A. Dagata

Precision Engineering Division, National Institute of Standards and Technology, Gaithersburg, Maryland 20899-8212

(Received 9 October 2003; accepted 1 March 2004; published 23 July 2004)

Oxide growth on sputter-deposited thin films is studied on the local scale by atomic force microscope (AFM)-assisted lithography. We investigate the group IV reactive metals Zr, Hf, Ti, and their nitrides. The nitrogen content of the deposition plasma affects the film crystal structure and electrical resistivity, which in turn alter the local oxidation rates. Mass transport plays an important role, producing features with heights ranging from a few nanometers up to *hundreds of nanometers*. The heights of the largest features are one to two orders of magnitude greater than observed in other material systems, and the growth is well controlled. We use various techniques to investigate the solid-state reaction and transport mechanisms involved in this oxidation driven by a highly localized electric field. Our results demonstrate the potential of AFM lithographic techniques for characterizing oxidation processes across a wide range of time and length scales. © 2004 American Vacuum Society. [DOI: 10.1116/1.1723269]

I. INTRODUCTION

This article concerns the low-temperature oxidation of thin (200 nm) metal and metal nitride films, where oxygen transport is driven by high local electric fields. The materials studied are Zr, Hf, and Ti, all of which act as reactive getter materials and have similar crystal structures. Atomic force microscope (AFM)-assisted lithography allows us to perform high-field localized anodization on these surfaces by applying small voltages (up to 30 V) between the tip and substrate. This technique provides us with a way to perform hyperthermal surface chemistry over a wide range of length and time scales. We can then use the oxide growth kinetics for materials characterization in combination with other techniques.

Recent investigations of the electrical currents involved in AFM lithography have significantly improved our understanding of the process,^{1,2} which can now be incorporated into existing models³⁻⁷ in a comprehensive way. It is important that models of AFM-assisted oxidation include the concepts developed previously for low-temperature oxide growth on larger length scales.⁸⁻¹⁰ For example, it is clear that a buildup of space-charge limits the growth of oxide features during anodic oxidation, and that the initial charge injection process is important for the short-time kinetics. The relative humidity also plays a major role in the formation of a water meniscus that serves as a source of hydroxyl ions that can oxidize the surface.

This article extends our previous work concerning the local oxidation kinetics of very thin (20 nm) Zr and ZrN_x films.^{11,12} Here, we discuss AFM-assisted oxide growth on 200-nm-thick films of Zr, Hf, Ti, and their nitrides. We find that changing the percentage of nitrogen in the sputtering gas changes the film deposition rate and affects the electrical resistivity and crystal structure of the resulting films, consistent with previous studies.¹³⁻²¹ We demonstrate that AFM oxidation kinetics are sensitive to these changes, and show that under appropriate conditions, we can form oxide structures that range from a few nanometers to *hundreds of nanometers* in height in a well-controlled manner.

The role of nitrogen in this process is important. We propose that nitrogen is responsible for suppressing the effects of space-charge buildup and for increasing the oxidation rate. Trends in our data suggest that the structural changes that occur in the films with the addition of nitrogen to the sputtering plasma are also accompanied by modifications of the electrical and mass transport properties of the films. The dependence of feature height on the nitrogen content of the sputtering plasma suggests that trapping sites for positive charges are modified by the presence of N in the films. To sustain the growth and produce such large structures, it is possible that nitrogen, once replaced in the lattice by oxygen, reacts with protons liberated from OH radicals during oxidation to form ammoniac species. These could leave the reaction zone and thereby suppress the effects of space-charge buildup. Mass transport is also important. We can grow these oxide structures at low relative humidity, and propose that

^{a)}Electronic mail: rex@uakron.edu

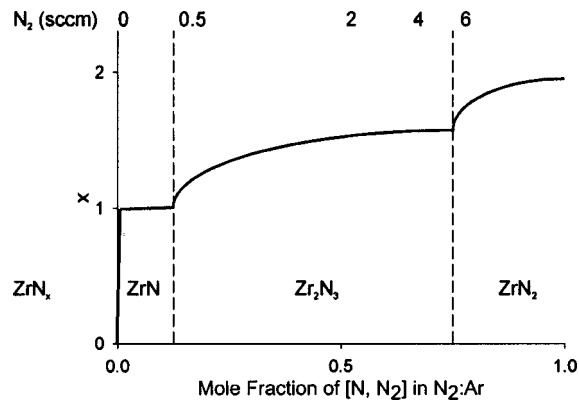


FIG. 1. Schematic illustration of the expected stoichiometry of zirconium nitride films vs the molar fraction of N and N_2 species in the sputtering gas. The nitrogen flow rates (sccm) used in this work are indicated. Similar behavior is expected for Hf and Ti. This illustration follows the data provided in Ref. 13.

subsurface (solid solution phase) oxygen can also participate in the oxidation process. These results are compatible with our previous studies of Zr surface chemistry,^{22–24} here, we extend the understanding of thermal and hyperthermal surface reactions on reactive metal surfaces by studying the Hf and Ti systems as well.

II. EXPERIMENT

Boron-doped ($1\text{--}3\ \Omega\text{cm}$) Si(111) wafers $500\text{--}550\ \mu\text{m}$ thick (Montco Silicon Technologies, Inc.) are cut into $1\ \text{cm}^2$ pieces and HF cleaned to serve as substrates for the thin films. Multiple substrates are placed into a physical vapor deposition chamber on a substrate holder 8 cm above the sputtering source. The substrate holder is earthed and there is no temperature control during deposition. The operational base pressure of the chamber is 8×10^{-4} Pa, and deposition rates are measured with a quartz crystal microbalance. The three metal sputtering targets used in this work were all acquired from Target Materials, Inc. The purity levels of the targets are given as Zr: 99.2%, Ti: 99.995%, and Hf: 99.5%. RF magnetron sputtering is performed at a power of 120 W in a background of argon between 0.29 and 0.51 Pa with an argon flow rate of 2 sccm. The targets are presputtered in argon (20 min, 5 sccm, 55 W) to remove surface oxides while a shutter shields the substrates. Nitrogen gas is introduced into the chamber for reactive sputtering at flow rates of 0.0, 0.5, 2, 4, and 6 sccm. Figure 1 schematically shows the relationship between these nitrogen flow rates and the expected film stoichiometry to calibrate the reader.¹³

AFM-assisted oxidation is performed under controlled ambient conditions at the National Institute for Standards and Technology (NIST) with a TopoMetrix Accurex II. We use contact mode techniques with W_2C -coated silicon cantilevers from Silicon-MDT Ltd. Relative humidity is varied in the range 6% to 55% using a glove box. The anodization time, applied dc voltage, and tip positioning are all computer controlled. For higher applied voltages, a constant voltage source is placed in series with the computer controlled volt-

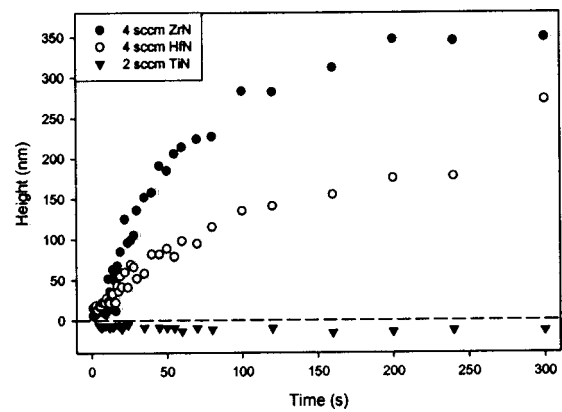


FIG. 2. Heights of oxide features vs time grown by AFM-assisted lithography on reactive metal nitride surfaces. The applied voltage is 30 V dc and the relative humidity 37%. Note the very large feature heights for zirconium and hafnium, as compared to the negative heights (i.e., holes) for titanium.

age output. With the tip stationary a potential difference is applied for a fixed amount of time. The tip is then moved to another location and the process repeated, so that we produce arrays of features. We subsequently image the features in contact mode with the same tips used for oxidation, and from these images extract height data. We use the same force-constant setpoint value for all experiments discussed here.

In-plane electrical resistivity measurements on the films use constant currents from $10\text{--}100\ \mu\text{A}$, and the measured potential differences are converted into resistivity values. The composition of the films is determined by x-ray photoelectron spectroscopy (XPS), and structural information is obtained by x-ray diffraction (XRD). Scanning electron microscopy (SEM), optical reflectivity, colorimetric, and microscopic evaluations of the films are also performed.

III. RESULTS AND DISCUSSION

Figure 2 shows height versus time data for AFM-assisted local oxide features grown on nitrated Zr, Hf, and Ti films under the same experimental conditions. Note the very large heights achieved with the Zr and Hf materials: *hundreds of nanometers*. These feature heights are one to two orders of magnitude larger than have been reported on any other substrate, and point to the unique properties of these reactive metal systems. Equally interesting are the Ti data, which show *negative* heights (i.e., “holes”). The formation of nanostructures, including holes, on Ti has been observed before.^{25–31} In the course of this study, we have devised a means to mitigate the dielectric breakdown of Ti that causes these holes, and to then grow positive-going structures. This procedure involves tip conditioning and forms the basis of future work. We present these data together in Fig. 2 only to demonstrate the significantly different behavior between Ti and that of Zr and Hf, which we will be discussing subsequently. The heights that we report are those measured directly from AFM images and are not corrected for expansion factors due to density differences between the oxides and the substrate.⁴

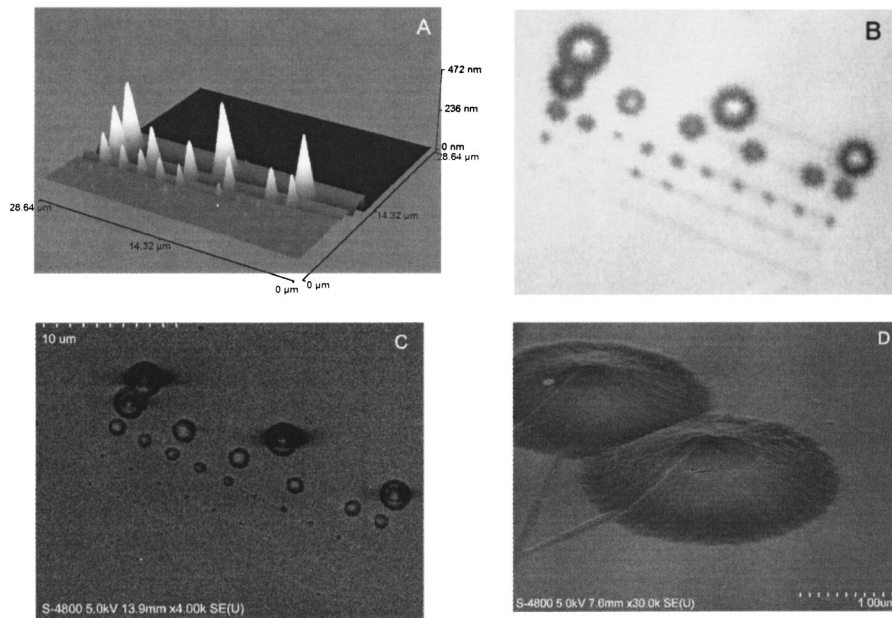


FIG. 3. Images of an array of oxide features grown by local anodization with an AFM tip on zirconium nitride (sputtered with a 4 sccm nitrogen flow rate). The applied voltage is 30 V dc, the relative humidity 33%, and the oxidation times vary from 1 to 300 s. The smallest features are formed at the shortest times, and successively larger features are grown at longer times. Panel A is an AFM image, panel B is an optical microscope image, and panels C and D are SEM images. Panel C in particular indicates the presence of insulating (center) and positively charged (perimeter) regions of the features.

Figure 3 shows the type of structures we are able to produce on these surfaces. Panel A is an AFM image of an array of oxide features grown on ZrN_x (4 sccm nitrogen flow rate in the sputtering gas) by applying 30 V dc for varying amounts of time (up to 300 s). Note the smooth, uniform profiles that indicate a well-controlled oxidation process, and the large sizes of the features grown at the longer times. Panel B of Fig. 3 is an *optical* microscope image of the same array. What we hope to impress on the readers with this panel is that AFM-assisted local oxidation can be used to transcend the nano- to micrometer-length scales under appropriate conditions with the proper choice of materials. This shows that we can acquire experimental data concerning oxidation kinetics under the same conditions that connect atomistic- and molecular-level models to continuum-level models.

Panels C and D of Fig. 3 are SEM images of the same oxide feature array. Note in panel C that the features emit secondary electrons differently depending on the region. The centers of most of the features appear bright, indicating that these regions are insulating and therefore charge during the imaging. The dark band around the perimeter of the features indicates a relatively lower secondary yield. This is the region of space-charge buildup, and is clearly distinct from the nearby zirconium nitride substrate. Panel D lends insight into the morphology of two of the larger oxide features, with what appear to be cracks on the right-hand side feature and a point defect on the left. The lines seen in Fig. 3 result from oxidation during the time the tip is being moved from location to location in the array. Here, the series dc power supply is left on to avoid transient spikes, and this produces nanoscale oxide lines since the growth kinetics are so rapid.

Figure 4 summarizes our findings for Zr and its nitrides. In panel A, we show how the height of the AFM-assisted oxide features depends on the nitrogen content of the sputtering plasma. Note that the maximum heights occur using a

4 sccm nitrogen flow rate in the sputtering gas for all three voltages and relative humidity values shown (see legend). These maxima correspond to a leveling off of the deposition rate (panel B), a maximum in the electrical resistivity (panel C), and a change in the crystal structure (panel D). These changes are consistent with published trends concerning nitride film growth in these materials systems.^{13–21}

Note in Figure 4, panel D, that the crystal structure changes from metallic, to crystalline nitride, to amorphous, to a higher nitride, and then to amorphous again. Refer to Fig. 1 for an illustration of how the nitrogen sccm values used in our experiments relate to expected film structure and stoichiometry.¹³ Our XPS data (not shown) are consistent with these trends, and we find that there is always oxygen in the films because of the gettering nature of these materials. It is interesting to note that for 0.5 sccm, the height of the oxide features (Fig. 4, panel A) produced on zirconium nitride is negative. In other words, these conditions form holes, similar to what is seen in Ti systems.

Comparing Fig. 4 (Zr) to Fig. 5 (Hf), we see similar behavior. For the hafnium system, the maximum oxide heights also occur for films grown with a nitrogen flow rate of 4 sccm, coincident with a low deposition rate, a high resistivity, and a higher nitride crystal structure. Subtle differences appear between the systems when we compare the actual oxide height values and crystal structure transition points, but overall the trends are the same. However, for Hf, we have no reproducible evidence for the formation of holes, unlike the cases of Ti (seen often) and Zr (only seen for 0.5 sccm nitrogen flow rate sputtering conditions). The fact that AFM oxidation kinetics reflect changes in structural and electrical properties of the films indicates that this technology has potential as a materials characterization tool on the local scale.

Our results demonstrate the influence that nitrogen can have on the oxidation of reactive metal films. Scanned probe

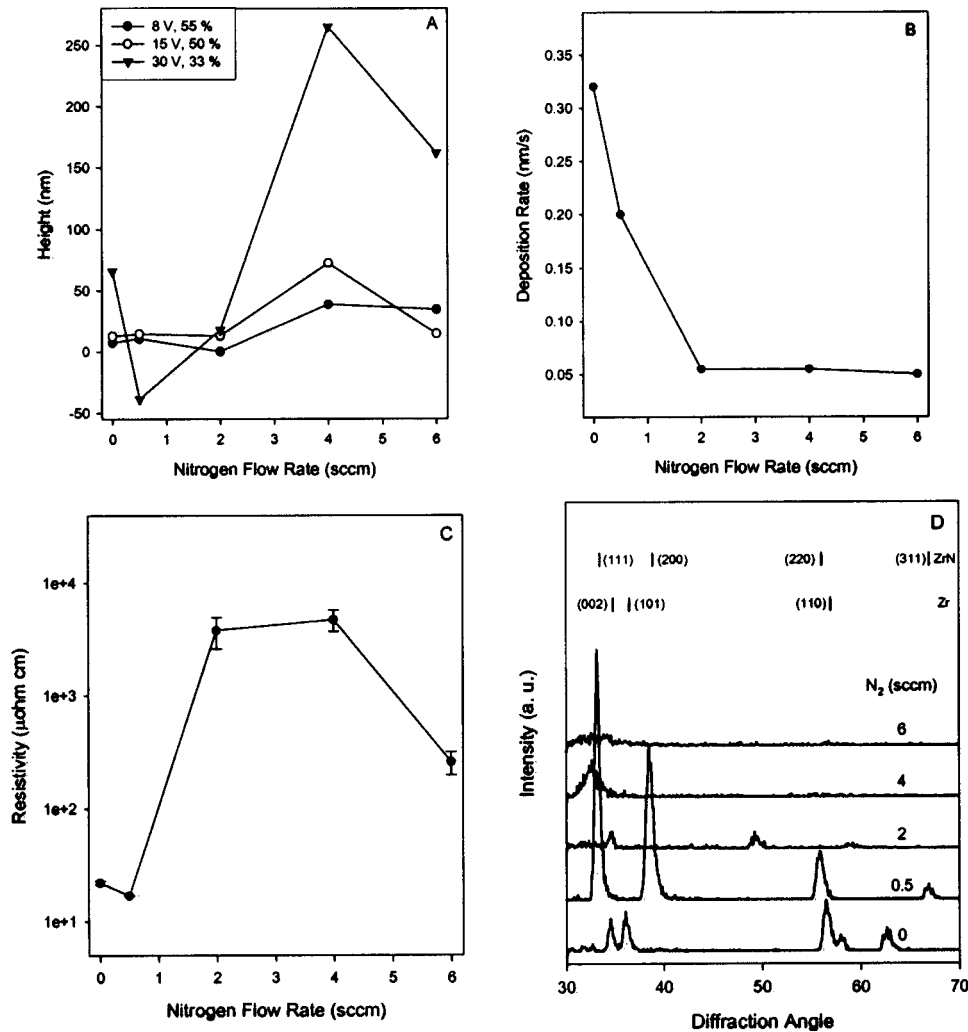


FIG. 4. Data from a series of zirconium nitride thin films. Panel A shows the heights of oxide features grown by AFM anodization at different applied voltages and relative humidity levels (see legend). Panel B shows the deposition rate of the zirconium nitride films, panel C contains the in-plane electrical resistivity of the as-grown films, and panel D provides their XRD patterns. Note how the maximum in oxide feature height (for films sputtered with a 4 sccm nitrogen flow rate) in panel A corresponds to a low deposition rate, high resistivity, and higher nitride crystal structure.

oxidation of silicon nitride has been performed previously;³² however, no significant enhancements in overall oxide height were found. Those authors were able to conclusively show that the nitride converts to oxide, and postulated N₂ evolution as a removal mechanism for the liberated nitrogen species. Although nitrogen evolution may also occur for the Zr and Hf nitrides, we cannot explain our very large feature heights without introducing additional mechanisms. These are that (1) liberated nitrogen reacts with hydrogen and escapes (possibly as ammonia), which suppresses the buildup of space-charge and allows for continued oxide growth; and (2) that mass transport of subsurface oxygen into the reaction zone, in combination with water from the meniscus, provides oxygen at a significantly higher rate than is available in other material systems.

It is important to point out that in some cases (e.g., Fig. 2), we are growing oxide features that are higher than the nitride films are thick. This necessitates rapid and sustained mass transport within the films, and a mechanism by which space-charge buildup is suppressed. The mechanisms proposed here for 200-nm-thick films are consistent with what we have discussed for 20-nm-thick zirconium nitride films.¹² In comparison with our previous work,¹² here, we increase

the sputtering power to shift the value of nitrogen flow rate necessary to reach the different structural transitions in these films.²¹ Gwo *et al.*²⁶ have reported that local oxidation of TiN results in TiO_xN_y structures, but they indicate no significantly large enhancements in feature height. It is plausible that the structures we have grown are also oxynitrides, and their stoichiometry is a subject of ongoing investigation.

Using the terminology of Fehlner and Mott,⁸ zirconium and hafnium in particular can be classified as having network-forming oxides. Since anion transport is the fundamental oxidation mechanism, the oxide growth rate is sensitive to the amount of oxygen present. These materials are known getters of oxygen, and we therefore expect enhanced oxide growth since the water meniscus and the subsurface regions of the film act in parallel to provide oxygen to the reaction zone. This is a reasonable interpretation of the fact that we can produce 30-nm-high oxide structures on zirconium nitride (4 sccm nitrogen flow rate during sputtering) films at a relative humidity of 6% (not shown), and grow features hundreds of nanometers high even at 33% relative humidity [Fig. 4(A)].

The changes in crystal structure observed in these materials as we increase the nitrogen content of the sputtering gas

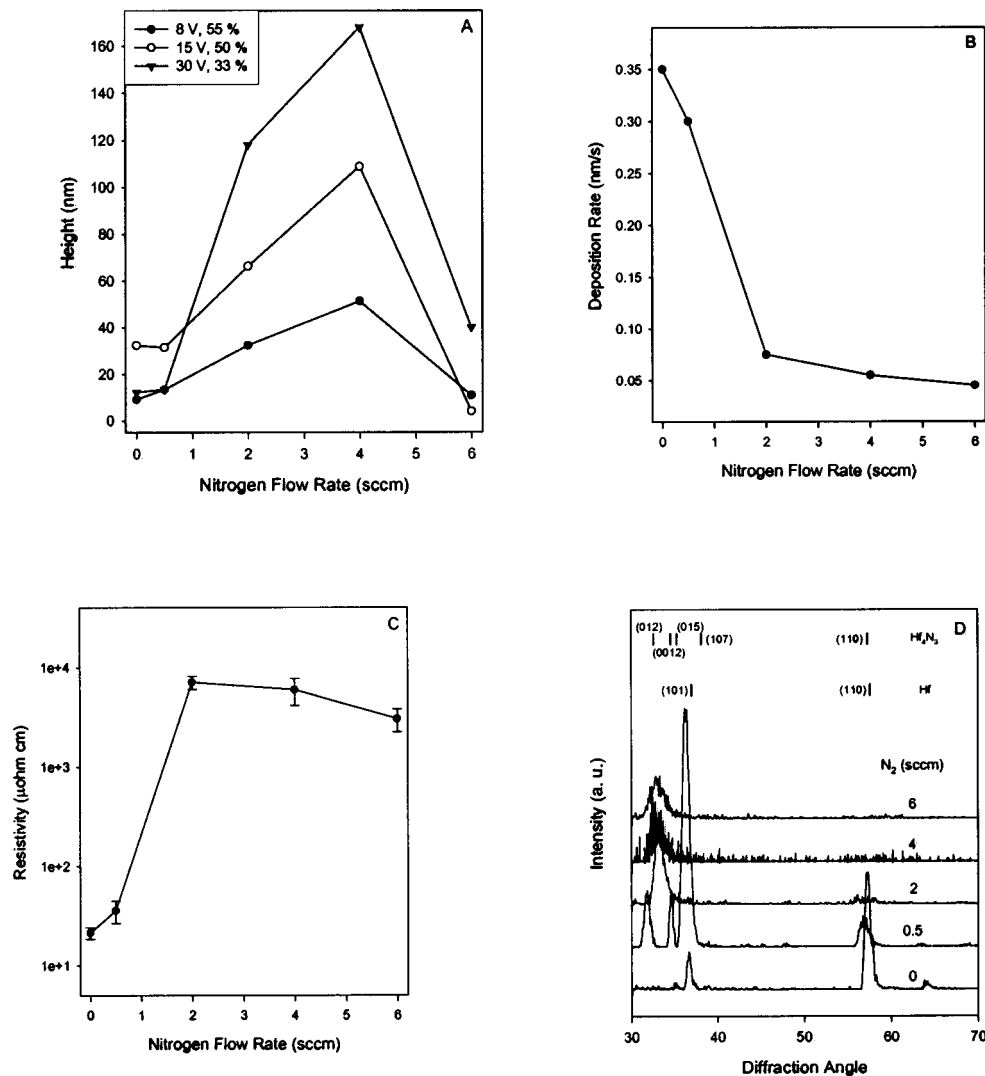


FIG. 5. Data from a series of hafnium nitride thin films. Panel A shows the heights of oxide features grown by AFM anodization at different applied voltages and relative humidity levels (see legend). Panel B shows the deposition rate of the hafnium nitride films, panel C contains the in-plane electrical resistivity of the as-grown films, and panel D provides their XRD patterns. Note how the maximum in oxide feature height (for films sputtered with a 4 sccm nitrogen flow rate) in panel A corresponds to a low deposition rate, high resistivity, and higher nitride crystal structure.

[Figs. 4(D) and 5(D)] alter the network for oxide formation. This probably changes the type and density of charge-trapping sites and the mass transport properties of the films, resulting in different oxide growth kinetics. There must be a competition between electrical and mass transport phenomena and the network-forming ability, since we see a maximum in the oxide feature heights with respect to nitrogen flow rate [Figs. 4(A) and 5(A)]. What is most promising is the sensitivity of the AFM-assisted growth process to these changes in film properties, and the fact that we can now produce nano- and micrometer-scale oxide structures. This allows us to study, in detail, oxidation processes over wide length and time scales. We anticipate that studies like these combined with comprehensive modeling schemes will enable scanning probe oxidation to be further developed as a materials characterization tool as well as a fundamental probe into hyperthermal surface chemistry.

IV. SUMMARY

We have discussed our recent results concerning low-temperature oxide growth on sputter-deposited thin films of Zr, Hf, Ti, and their nitrides. Using AFM-assisted lithographic techniques, we are able to control the applied electric field and relative humidity, and to study the oxidation process on a local scale. The nitrogen content of the film deposition plasma affects the resulting crystal structure and electrical resistivity, which are reflected in the local oxidation kinetics. We produce features with heights ranging from a few nanometers up to *hundreds of nanometers*, the latter being one to two orders of magnitude larger than observed in other material systems. Most importantly, the growth is well controlled. We therefore demonstrate the potential of scanned probe lithography as a materials characterization tool that spans a wide range of time and length scales.

ACKNOWLEDGMENTS

Acknowledgment is made to the Donors of the American Chemical Society Petroleum Research Fund for partial support of this research. Support from the NIST Office of Microelectronics Programs is also acknowledged. We would like to thank Dr. Wayne Jennings of the Case Western Reserve University Center for Surface Analysis of Materials, and Dr. Andras Vladar of NIST, for their technical advice and assistance. Disclaimer: Certain commercial equipment is identified in this article in order to describe the experimental procedure adequately. Such description does not imply recommendation or endorsement by NIST, nor does it imply that the equipment identified is necessarily the best available for the purpose.

- ¹F. Perez-Murano, C. Martin, N. Barniol, H. Kuramochi, H. Yokoyama, and J. A. Dagata, *Appl. Phys. Lett.* **82**, 3086 (2003).
²H. Kuramochi, F. Perez-Murano, J. A. Dagata, and H. Yokoyama, *Nanotechnology* **15**, 297 (2004).
³J. A. Dagata, T. Inoue, J. Itoh, K. Matsumoto, and H. Yokoyama, *J. Appl. Phys.* **84**, 6891 (1998).
⁴E. Dubois and J.-L. Bubendorff, *J. Appl. Phys.* **87**, 8148 (2000).
⁵E. S. Snow, G. G. Jernigan, and P. M. Campbell, *Appl. Phys. Lett.* **76**, 1782 (2000).
⁶J. A. Dagata, F. Perez-Murano, G. Abadal, K. Morimoto, T. Inoue, J. Itoh, and H. Yokoyama, *Appl. Phys. Lett.* **76**, 2710 (2000).
⁷K. Morimoto, F. Pérez-Murano, and J. A. Dagata, *Appl. Surf. Sci.* **158**, 205 (2000).
⁸F. P. Fehlner and N. F. Mott, *Oxid. Met.* **2**, 59 (1970).
⁹F. P. Fehlner, *Philos. Mag. B* **55**, 633 (1987).
¹⁰J. A. Davies, B. Domeij, J. P. S. Pringle, and F. Brown, *J. Electrochem. Soc.* **112**, 675 (1965).
¹¹N. Farkas, G. Zhang, E. A. Evans, R. D. Ramsier, and J. A. Dagata, *J. Vac. Sci. Technol. A* **21**, 1188 (2003).

- ¹²N. Farkas, G. Zhang, K. M. Donnelly, E. A. Evans, R. D. Ramsier, and J. A. Dagata, *Thin Solid Films* **447-448**, 468 (2004).
¹³M. Wautelet, J. P. Dauchot, F. Debal, S. Edart, and M. Hecq, *J. Mater. Res.* **11**, 825 (1996).
¹⁴H. M. Benia, M. Guemmaz, G. Schmerber, A. Mosser, and J.-C. Parlebas, *Appl. Surf. Sci.* **200**, 231 (2002).
¹⁵H. M. Benia, M. Guemmaz, G. Schmerber, A. Mosser, and J.-C. Parlebas, *Appl. Surf. Sci.* **211**, 146 (2003).
¹⁶L. Pichon, A. Straboni, T. Girardeau, M. Drouet, and P. Widmayer, *J. Appl. Phys.* **87**, 925 (2000).
¹⁷B. O. Johansson, U. Helmersson, M. K. Hibbs, and J.-E. Sundgren, *J. Appl. Phys.* **58**, 3104 (1985).
¹⁸B. O. Johansson, J.-E. Sundgren, and U. Helmersson, *J. Appl. Phys.* **58**, 3112 (1985).
¹⁹C. Friedrich, G. Berg, E. Broszeit, and K.-H. Kloos, *Surf. Coat. Technol.* **74-75**, 279 (1995).
²⁰S. Shinkai and K. Sasaki, *Jpn. J. Appl. Phys.* **38**, 2097 (1999).
²¹C.-P. Liu and H.-G. Yang, *Mater. Res. Soc. Symp. Proc.* **721**, 117 (2002).
²²S. Ankrah, Y. C. Kang, and R. D. Ramsier, *J. Phys.: Condens. Matter* **15**, 1899 (2003).
²³N. Stojilovic, Y. C. Kang, and R. D. Ramsier, *Surf. Interface Anal.* **33**, 945 (2002).
²⁴Y. C. Kang and R. D. Ramsier, *Surf. Sci.* **519**, 229 (2002).
²⁵S. Melinte, B. Nysten, and V. Bayot, *Superlattices Microstruct.* **24**, 79 (1998).
²⁶S. Gwo, C.-L. Yeh, P.-F. Chen, Y.-C. Chou, T. T. Chen, T.-S. Chao, S.-F. Hu, and T.-Y. Huang, *Appl. Phys. Lett.* **74**, 1090 (1999).
²⁷R. Held, T. Heinzel, P. Studerus, and K. Ensslin, *Physica E (Amsterdam)* **2**, 748 (1998).
²⁸K. Unal, B.-O. Aronsson, Y. Mugnier, and P. Descouts, *Surf. Interface Anal.* **34**, 490 (2002).
²⁹S. Lemesenko, S. Gavrilov, V. Shevyakov, V. Roschin, and R. Solomatenko, *Nanotechnology* **12**, 273 (2001).
³⁰C. Galli, M. C. Coen, R. Hauert, V. L. Katanaev, M. P. Wymann, P. Groning, and L. Schlapbach, *Surf. Sci.* **474**, L180 (2001).
³¹C. Huh and S.-J. Park, *J. Vac. Sci. Technol. B* **18**, 55 (2000).
³²R. Klauser, I.-H. Hong, H.-J. Su, T. T. Chen, S. Gwo, S.-C. Wang, T.-J. Chuang, and V. A. Gritsenko, *Appl. Phys. Lett.* **79**, 3143 (2001).